Analyzing the interpretative ability of landscape pattern to explain thermal environmental effects in the Beijing-Tianjin-Hebei urban agglomeration

Dongchuan Wang [Corresp., 1, 2] , **Zhichao Sun** [1] , **Junhe Chen** [1] , **Xiao Wang** [1] , **Xian Zhang** [1] , **Wei Zhang** [1]

[1] School of Geology and Geomatics, Tianjin Chengjian University, Tianjin, China

[2] Tianjin Key Laboratory of Civil Structure Protection and Reinforcement, Tianjin, China

Corresponding Author: Dongchuan Wang
Email address: wangdongchuan@tcu.edu.cn

The development of the urban agglomeration has caused drastic changes in landscape pattern and increased anthropogenic heat emission and lead to the urban heat island (UHI) effect more serious. Therefore, understanding the interpretation ability of landscape pattern on the thermal environment has gradually become an important focus. In the study, the spatial heterogeneity of the surface temperature was analyzed using the hot-spot analysis method which was improved by changing the calculation of space weight. Then the interpretation ability of a single landscape and a combination of landscapes to explain surface temperature was explored using the Pearson correlation coefficient and ordinary least squares (OLS) regression from different spatial levels, and the spatial heterogeneity of the interpretation ability was explored using geographical weighted regression (GWR) under the optimal granularity (5 km × 5 km). The results showed that: (1) The hot spots of surface temperature were distributed mainly in the plains and on the southeast hills, where the landscapes primarily include ArtLS and FarmLS. The cold spots were distributed mainly in the northern hills, which are dominated by ForLS. (2) On the whole, the interpretative ability of ForLS, FarmLS, ArtLS, GreenLSP and EcoLSP to explain surface temperature was stronger, whereas the interpretative ability of GraLS and WetLS to explain surface temperature was weaker. The interpretation ability of landscape pattern to explain surface temperature was obviously different in different areas. Specifically, the ability was stronger in the hills than in the plain and plateau. The results are intended to provide scientific basis for adjusting landscape structural, optimizing landscape patterns, alleviating the UHI effect and coordinating the balance among cities within the urban agglomeration.

1 **Analyzing the interpretative ability of landscape pattern to explain thermal environmental**

2 **effects in the Beijing-Tianjin-Hebei urban agglomeration**

3 **Dongchuan Wang[1, 2], Zhichao Sun[1], Junhe Chen[1], Xiao Wang[1], Xian Zhang[1], Wei Zhang[1]**

4 [1]School of Geology and Geomatics, Tianjin Chengjian University, Tianjin, China

5 [2]Tianjin Key Laboratory of Civil Structure Protection and Reinforcement, Tianjin, China

6 Corresponding Author:

7 Dongchuan Wang[1,2]

8 No. 26 Jinjing RD, Xiqing District, Tianjin, 300384, China

9 Email address: wangdongchuan@tcu.edu.cn

10 **Abstract**

11 The development of the urban agglomeration has caused drastic changes in landscape pattern and

12 increased anthropogenic heat emission and lead to the urban heat island (UHI) effect more

13 serious. Therefore, understanding the interpretation ability of landscape pattern on the thermal

14 environment has gradually become an important focus. In the study, the spatial heterogeneity of

15 the surface temperature was analyzed using the hot-spot analysis method which was improved by

16 changing the calculation of space weight. Then the interpretation ability of a single landscape

17 and a combination of landscapes to explain surface temperature was explored using the Pearson

18 correlation coefficient and ordinary least squares (OLS) regression from different spatial levels,

19 and the spatial heterogeneity of the interpretation ability was explored using geographical

20 weighted regression (GWR) under the optimal granularity (5 km × 5 km). The results showed

21 that: (1) The hot spots of surface temperature were distributed mainly in the plains and on the

22 southeast hills, where the landscapes primarily include ArtLS and FarmLS. The cold spots were

23 distributed mainly in the northern hills, which are dominated by ForLS. (2) On the whole, the

24 interpretative ability of ForLS, FarmLS, ArtLS, GreenLSP and EcoLSP to explain surface

25 temperature was stronger, whereas the interpretative ability of GraLS and WetLS to explain

26 surface temperature was weaker. The interpretation ability of landscape pattern to explain

27 surface temperature was obviously different in different areas. Specifically, the ability was

28 stronger in the hills than in the plain and plateau. The results are intended to provide scientific

29 basis for adjusting landscape structural, optimizing landscape patterns, alleviating the UHI effect

30 and coordinating the balance among cities within the urban agglomeration.

31 **Keywords**: Beijing-Tianjin-Hebei urban agglomeration; landscape pattern; surface temperature;

32 the interpretative ability; spatial heterogeneity

33 **1 Introduction**

34   In recent years, because of the rapid development of urbanization, artificial landscape has
35 gradually eroded the natural landscape (Su et al., 2012; Angel et al., 2011; Miao et al., 2011).
36 Impermeable layers with high thermal conductivity which are composed of cement and asphalt
37 continue to expand, and energy and material consumption keep increasing which lead to
38 greenhouse gas and anthropogenic heat emissions increasing (Bonafoni et al., 2017; Barrington-
39 Leigh et al., 2015). This has changed the heat flow and heat balance between atmosphere and
40 land surface, aggravated the heat island effect, and has seriously threatened the urban living
41 environment and the quality of life for dwellers (Zhang et al., 2009; Gu et al., 2016). Therefore,
42 the search for mitigation methods of urban heat island effect has become a hot research topic
43 among scholars (Connors et al., 2013).
44   Most previous studies have looked for ways to mitigate the heat island effect from its causes
45 and have shown that factors, such as surface parameters, human activities, altitude, and average
46 wind speed, are significantly correlated with the urban thermal pattern (Amiri et al., 2009; Du et
47 al., 2016; Jiao et al., 2019). Many studies have shown that there is a significant correlation
48 between the Normalized Difference Vegetation Index (NDVI), the Normalized Difference Built-
49 up Index (NDBI) and the Normalized Difference Water Index (NDWI) and surface temperature,
50 and the surface parameters are the main cause of heat island problems (Zhao et al., 2018; Xiao et
51 al., 2007; Chen et al., 2006), which are closely related to landscape patterns of the underlying
52 surface (Gage et al., 2017; Zullo et al., 2018). Therefore, the study on the coupling relationship
53 between landscape pattern and surface temperature is the breakthrough to alleviate the urban heat
54 island effect (Li et al., 2017; Li et al., 2011).
55   Since the landscape pattern index can accurately reflect the spatial pattern information of
56 the landscape (Zhao et al., 2018; Zhao et al., 2018), the Pearson correlation coefficient and
57 ordinary least squares regression method can reflect the relationship between different factors(Yi
58 et al., 2018; Asgarian et al., 2018; Connors et al., 2013). Therefore, following these methods,
59 more and more studies had been conducted to explore the relationship between landscape pattern
60 and surface temperature. These studies have shown that the correlation between landscape area
61 percentage index (PLAND) and surface temperature was more   significant than patch density
62 (PD), edge density (ED), landscape shape index (LSI), and the relationship between the PLAND
63 of different landscapes and surface temperatures also was different (Chen et al., 2012). For
64 example, increasing the area of forest landscape and wetland landscape could achieve a cooling
65 effect (Kumar et al., 2015; Xiao et al., 2018), and increasing the area of artificial landscape could
66 lead to an increase in surface temperature (Jones et al., 1990). In addition, the relationship
67 between the PLAND of same landscape and surface temperature varied in different regions and
68 scales (Shen et al., 2015). This difference was related not only to the heterogeneity of the
69 landscape pattern but also to the granularity of the selected analytical window (Guo et al., 2012;
70 Lu et al., 2018; Estoque et al., 2017). However, the current study on the interpretation ability of
71 integrated landscapes such as ecological land (composed of forestland, grassland and wetland) to
72 explain surface temperature is insufficient. In addition, some progress has been made in

exploring the spatial heterogeneity of the interpretation ability of landscape pattern to explain surface temperature, but the research revealed the causes of the spatial heterogeneity from the comprehensively perspective including landscape, topography, landform, elevation difference, microclimate difference, and human activities need greater progress (Zhou et al., 2011). When exploring the heterogeneity of the relationship between the two variables, the ordinary least squares (OLS) is not applicable to reflect the spatial heterogeneity of the relationship between the dependent variable and independent variables space difference, geographically weighted regression (GWR) is a kind of effective method to reflect the spatial heterogeneity, and Li et al. (2010) found that GWR than OLS provides a better fitting and more localized information when researching the landscape driving factors of LST.

At present, most studies had made significant progress in clarifying the thermal environment problems of single cities or of a few large cities, such as Beijing and Shanghai (Wang et al., 2017). With the development and integration of the city,in the Beijing-Tianjin-Hebei urban agglomeration, Yangtze River Delta urban agglomeration, Pearl River Delta urban agglomeration, and other large-scale regions, the research on the thermal environment should deserve further attention (Zhou et al., 2018).. As the main form of promoting urbanization in China, urban agglomeration has a close spatial structure and close economic ties. And as the distance between cities decreased, high-temperature regions continuously integrated and expanded, which contributed to the urban heat island effect becoming increasingly serious. In addition, at the 18th National Congress of the Communist Party of China and in the coordinated development strategy of Beijing-Tianjin-Hebei, it was emphasized that development of urban agglomerations is considered to be comprehensive, healthy, coordinated, and sustainable development. Thus, we need to pay more attention to the problem of the thermal environment in the Beijing-Tianjin-Hebei urban agglomeration.

From the perspective of sustainable and integrated development in Beijing-Tianjin-Hebei urban agglomeration integration, we combined data for surface temperature and normalized difference vegetation index (NDVI) in summer 2015, land cover, digital elevation model (DEM), and topography. In the paper, the determination of Euclidean distance was improved from two to three dimensions, which was included in the hot-spot analysis method, and the spatial pattern information of landscapes and surface temperatures were analyzed quantitatively. To explore the optimal analytical window granularity of the relationship between landscape pattern and surface temperature on for an urban agglomeration, we applied the Pearson correlation coefficient. Then, we combined OLS and GWR models to explain the influence and the interpretative ability of landscape pattern to explain surface temperature and their spatial heterogeneity from different spatial levels. Finally, we revealed the origin of the spatial heterogeneity from the landscapes of the basement, topography, elevation, and human activities. These results provide a scientific basis for the adjustment of land cover structure and a reference to improve the thermal environment in the Beijing-Tianjin-Hebei urban agglomeration.

2 Methodology

2.1 Study area

The Beijing-Tianjin-Hebei urban agglomeration is composed of Beijing, Tianjin, and 11 cities in Hebei Province (Figure 1), which is located in north latitude 36°05'~42°40', the area is 216485.2 km², the area of land for construction is about 25000 km², accounting for 11.6% which is significantly higher than the national average. According to the data of The Sixth National Census, the permanent population was 104 million in 2010, with a population density of 484 inhab/km². The city with the highest population density is Beijing, with 1167 inhab/km². The city with the lowest population density is Hebei province, with 381 inhab/km².

The terrain is complex and the difference in elevation is significant. The terrain includes hills, plains, intermontane basins, and other types of terrain; plains and hills are the primary types of terrain. The plains are dominated by the northern China plain, which is concentrated in the eastern part of the Beijing-Tianjin-Hebei urban agglomeration. Hills are found primarily in the northwest region of the Beijing-Tianjin-Hebei urban agglomeration (Zhangjiakou and Chengde) and in the north of Baoding city, which mainly includes the Taihang, Yanshan, and Jundu mountains, and forest is the main landscape. The climate is a temperate continental climate, with severe cold in the winter and heat in the summer. The annual temperature is quite varied, so the vegetation type is primarily temperate deciduous broad-leaved forest, which is affected significantly by the climate (Li et al., 2017; Miao et al., 2015; Zhang et al., 2017).

Figure.1 Location and hillshade of the Beijing-Tianjin-Hebei urban agglomeration

2.2 Data source and preprocessing

The data used in this study mainly included land cover, DEM, surface temperature, topography and NDVI data for the Beijing-Tianjin-Hebei urban agglomeration (Table 1). We obtained the land cover data from the Landsat8 OLI remote-sensing images (2015) with cloud cover less than 5% after manual visual interpretation. The resolution of the land cover data is 30m×30m. The land cover types that we interpreted included forest, grassland, wetland, farmland, artificial surface, and bare land. We verified the accuracy of the interpretation using historical data and field investigation during the same period, and the accuracy was higher than 93%.

The northern and southern latitude span is large in the Beijing-Tianjin-Hebei urban agglomeration. To reduce the influence of latitude position, seasonal change, and cloud cover on the accuracy of the relationship between landscape pattern and surface temperature, we selected surface temperature synthetic products (MOD11A2) in four phases (July 4, July 12, July 20, July 28, 2015) and vegetation index synthetic products (MOD13A1) in two phases(July 12 and July 28, 2015) which always were used to reflect surface temperature and NDVI in larger areas (Ferreira et al., 2013; Chen et al., 2011). First of all, we extracted "LST_Day_1km" and "NDVI"

147 from the data of two products using ENVI 5.3. Then, we preprocessed and averaged these
148 products. Finally we obtained average surface temperature data and average NDVI data for the
149 Beijing-Tianjin-Hebei urban agglomeration for July 2015. The resolution of the two data is
150 1000m×1000m, 500m×500m respectively.
151   The vector data sources for topography included 10 types of topography, including alluvial
152 fan, alluvial fan, marine plain, yellow pan plain, flood plain, depression, mountain, hill,
153 intermontane basin, and plateau.
154
155   Table.1 Data sources

156 **2.3 Methods**

157   The process in this study consists of five steps: firstly, classifying landscape types according
158 to primary classification results of land cover and constructing landscape pattern; secondly,
159 dividing the study area according to terrain; thirdly, expressing the spatial information of surface
160 temperature using the improved hot-spot analysis method; fourthly, exploring the optimal
161 analytical window granularity of the relationship between landscape pattern and surface
162 temperature using the Pearson correlation analysis method; finally, studying the interpretative
163 ability of landscape pattern to explain surface temperature using OLS and GWR from different
164 spatial levels. The flow chart of this study is shown in Figure 2.
165
166   Figure.2 The flowchart of the paper structure

167 **2.3.1 Classification of landscape**

168   Previous research has shown that the relationship between a single landscape and surface
169 temperature has been well studied (Zhao et al., 2018). In real life, however, the surface
170 temperature is the result of the mutual influence of various landscapes. Therefore, we explored
171 the relationship between surface temperature and two kinds of integrated landscape pattern , as
172 well as a single landscape.
173   Since the change of landscape pattern is related to human activities(Li et al.,2016), we
174 divided the landscapes of the Beijing-Tianjin-Hebei urban agglomeration into six landscapes
175 according to the degree of human influence on the landscape shaping process and primary
176 classification results of land cover: (1) Forest landscape (ForLS), mainly referring to the forest
177 land in the land cover classification; (2) Grassland landscape (GraLS), mainly referring to
178 grassland in the land cover classification; (3) Wetland landscape (WetLS), mainly referring to
179 rivers, lakes and other water areas in the land cover classification; (4) Farmland landscape
180 (FarmLS), mainly referring to cultivated land in land cover classification; (5) Artificial landscape
181 (ArtLS), mainly referring to the artificial surface in land cover classification; (6) Bare land
182 landscape (BareLS), mainly referring to the unused land in the land cover classification.

183 Ecological landscape refers to the types of land cover mainly providing ecosystem services,
184 including forest, garden, grassland, water area, wetland and other natural land, such as glacier.
185 Green landscape generally refers to the area with green plants, including park green space,
186 production green space and protection green space and so on where NDVI values tend to be high.
187 Therefore, in this study, landscapes were intergrated into two kind of patterns, the Ecological
188 landscape pattern (EcoLSP, made up of three kinds of landscapes, ForLS, GraLS, and WetLS)
189 and Green space landscape pattern (GreenLSP), which was expressed using NDVI. In the study,
190 we used all the single landscapes and integrated landscape patterns to explore the relationship
191 between landscape pattern and surface temperature using the Pearson correlation analysis
192 method and OLS regression method.

193 **2.3.2 Division of study area according to terrain**

194   In mountainous areas with complex environmental conditions, key topographic factors, such
195 as altitude and slope, have a significant impact on surface temperature (Jiao et al., 2019; Duan et
196 al., 2015). The terrain in the Beijing-Tianjin-Hebei urban agglomeration is complex, including
197 hills that include the Taihang, Yanshan, and Jundu mountains and parts of the northern China
198 plain, with significant differences in elevation between these different types of terrain.
199   To explore the influence of altitude on surface temperature, based on the grid of 1 km × 1
200 km, we statistically analyzed the average surface temperature and average DEM values in
201 different grids. We found a significant correlation between altitude and surface temperature
202 using the Pearson correlation analysis method (the correlation coefficient was −0.68**). To
203 reduce the influence of topographic factors on the relationship between landscape pattern and
204 surface temperature, we divided the region in the Beijing-Tianjin-Hebei urban agglomeration
205 into three types of terrain—plain, hills and plateau (Figure 3).
206
207   Figure.3 Terrains and elevation of the Beijing-Tianjin-Hebei urban agglomeration

208 **2.3.3 Spatial information expression of surface temperature**

209   The $Getis\text{-}Ord\ G_i^*$ local hot-spot analysis method can be used to identify the spatial

210 clustering regions with high value and low value of statistical significance. Therefore, in this part,
211 we used this method to carry out clustering analysis and spatial heterogeneity expression of
212 surface temperature. We combined the results of the hot-spot analysis with the landscape pattern
213 and terrain to reveal landscape composition information for hot and cold spots in different types

214 of terrain in this region. The formula of $Getis\text{-}Ord\ G_i^*$ (Feng et al., 2017) was as follows:

215
$$G^*_i = \frac{\sum_{j=1}^{n} w_{ij} x_j - \bar{x} \sum_{j=1}^{n} w_{ij}}{\sqrt{\frac{\sum_{j=1}^{n} x_j^2}{n} - \bar{x}^2} \sqrt{\frac{\left[n\sum_{j=1}^{n} w_{ij}^2 - \left(\sum_{j=1}^{n} w_{ij}\right)^2\right]}{n-1}}},$$
(1)

216 where n represents the total number of factors in the study area; w_{ij} is the spatial weight

217 coefficient between the factor i and factor j, reflecting the spatial relationship; x_j is the attribute

218 value of the factor j; and $\bar{x}$ is the average attribute value of n factors.

219 The method to determine the spatial weight coefficient is the key to determining the degree

220 of influence between two factors. In this part, we selected the inverse distance weighting method

221 to calculate the spatial weight coefficient. The traditional inverse distance weighting method was

222 constructed primarily in the two-dimensional coordinate system. In hills, however, altitude has a

223 significant impact on the Euclidean distance between two points. Therefore, we combined DEM

224 data and the two-dimensional coordinate system to construct the three-dimensional coordinate

225 system to calculate the distance and weight in the three-dimensional coordinate system. The

226 formula of w_{ij} follows:

227
$$w_{ij} = \frac{\left((X_j - X_i)^2 + (Y_j - Y_i)^2 + (Z_j - Z_i)^2\right)^{-\frac{p}{2}}}{\sum_{a=1}^{m} \left((X_j - X_i)^2 + (Y_j - Y_i)^2 + (Z_j - Z_i)^2\right)^{-\frac{p}{2}}} (i \neq j),$$
(2)

228 where m represents the total number of factors in the local neighborhood of factor i, and it is 8

229 according to the best practice criterion; X_j, Y_j, and Z_j are the X, Y, and Z coordinate values of the

230 factor j; X_i, Y_i, and Z_i are the X, Y, and Z coordinate values of the factor i; and p is the parameter,

231 which is determined by the minimum value of the root mean square error, where it is 2. To avoid

232 the situation in which the distance between two elements is 0, $w_{ij} = 1$ when $i = j$.

233 Z score, p values, and confidence level can reflect a statistically significant aggregation or

234 discrete model of factors or the value. The z-score ($Z(G_i^*)$) is the statistic of G_i^*, which is a

235 multiple of the standard deviation; p is the probability. The relationship among the three is

236 shown in Table 2, and the relevant contents in the table refer to the help document of ArcGIS

237 10.2 software. The formula of $Z(G_i^*)$ is as follows:

238
$$Z(G_i^*) = \frac{1 - E(G_i^*)}{\sqrt{VAR(G_i^*)}},$$
(3)

239 where $E(G_i^*)$ is the expected value of the local exponent of $Getis\text{-}Ord\ G_i^*$; and $VAR(G_i^*)$ is

240   the variance of the local exponent of $Getis\text{-}Ord\ G_i{}^*$.

241

242   Table.2 Z score, p value, confidence level, and explanation

243   **2.3.4 Exploration of the optimal analytical window granularity of the relationship between**

244   **landscape pattern and surface temperature**

245   The relationship between surface temperature and landscape pattern is correlated
246   significantly with the analytical window granularity. If the analytical window granularity is too
247   small, the calculation will be too large, the information of landscape pattern inside the window
248   will be single, and the excessive analytical window granularity will affect the full embodiment of
249   heterogeneity (Estoque et al., 2017). Therefore, based on the resolution of surface temperature
250   data (1 km × 1 km), we selected eight kinds of analytical window granularity, including 1 km × 1
251   km, 3 km × 3 km, 5 km × 5 km, 7 km × 7 km, 9 km × 9 km, 11 km × 11 km, 13 km × 13 km, and
252   15 km × 15 km, and explored the optimal analytical window granularity of the relationship
253   between landscape pattern and surface temperature in the Beijing-Tianjin-Hebei urban
254   agglomeration.
255   Following the principle of grid statistical analysis, we divided the research area into
256   multiple grids. On the basis of this principle, we then analyzed the average temperature, the
257   PLAND of different landscapes and the average NDVI for each grid. Therefore, the phenomenon
258   that the resolution of basic data was not identical has little effect on our research results.
259   We used the Pearson correlation analysis method to express the relationship between two
260   factors by observing the correlation coefficient r (Lu et al., 2018; Miao et al., 2010). We
261   determined the analytical window granularity by comparing r^2.

262   **2.3.5 Interpretative ability of landscape pattern to explain surface temperature**

263   On the basis of the optimal analytical window granularity, we combined OLS and GWR
264   model to explore the interpretative ability and degree of influence of landscape pattern on surface
265   temperature from different spatial levels.
266   The OLS model reflected the positive and negative relationship between the interpretative
267   variables and explained the variable and the strength of the relationship by the regression
268   coefficient (β). The R^2 of the results reflected the fitting effect of the evaluation model. The
269   formula of the regression model and R^2 (Farahani et al., 2010) is as follows:

270                           $$y_i = \beta_0 + \beta x_i + \varepsilon_i, \text{ and}$$ (4)

271
$$R^2 = \left(\frac{\sum_{i=1}^{n}(x_i - \bar{x})(y_i - \bar{y})}{\sqrt{\sum_{i=1}^{n}(x_i - \bar{x})^2} \sqrt{\sum_{i=1}^{n}(y_i - \bar{y})^2}} \right)^2. \tag{5}$$

272   In formula (4), y_i represents the explained variable value of the sampling point i; x_i represents

273   the interpretative variable value of the sampling point i; β_0 is the intercept, and β is the slope or

274   regression coefficient of the interpretative variable; and ε_i is the residual. In formula (5), the

275   means of x_i and y_i are the same as the means in formula (4), $\bar{x}$ represents the average value of

276   the interpretative variable, $\bar{y}$ represents the average value of the explained variable, and n
277   represents the total number of explained variables.
278   Although the OLS model can express the interpretative ability of landscape pattern to
279   explain surface temperature as a whole, it cannot accurately reflect the spatial heterogeneity. On
280   the basis of OLS model and GWR model, we incorporated spatial characteristics of the data and
281   used subsamples from nearby observations to estimate each point in the study area. The
282   regression results reflected the spatial heterogeneity of the interpretative ability and the degree of
283   influence. The GWR formula (Guo et al.,2008; Zhao et al., 2018) is as follows:

284
$$y_i = \beta_0(u_i, v_i) + \sum_{k=1}^{p} \beta_k(u_i, v_i)x_{ik} + \varepsilon_i, \tag{6}$$

285   where y_i represents the value of the explained variable of the sampling point i, x_{ik} represents the
286   value of the interpretative variable k at the sampling point i, (u_i, v_i) represents the coordinates of
287   the sampling point i, $\beta_0(u_i, v_i)$ represents the statistical regression constant of the sampling point
288   i, $\beta_k(u_i, v_i)$ represents the regression coefficient k of the sampling point i, its purpose is to
289   estimate the adjacent space observations, p is the number of variables participating in the
290   regression at a sampling point, and ε_i is the residual. We adopted the kernel function for the
291   estimation function of $\beta_k(u_i, v_i)$, and the following formula of $\beta_k(u_i, v_i)$:

292
$$\beta_k(u_i, v_i) = \left(X^T W(u_i, v_i)X \right)^{-1} X^T W(u_i, v_i)y, \tag{7}$$

293   where X and X^T is the matrix and transpose of the factor values in the neighborhood of the

294   observation point (u_i, v_i); and $W(u_i, v_i)$ represents the distance weight matrix of the observation

295   point (u_i, v_i), which is the observation function between the observation point and other points

296   and is composed of factor W_{ij} in the distance weight matrix. The formula of W_{ij} is as follows:

297
$$W_{ij} = \exp\left(-\frac{d_{ij}^2}{h^2}\right), \qquad (8)$$

298   where h is the kernel bandwidth; and d_{ij} is the distance between the observation point i and the

299   factors j in the neighborhood. In this study, we used Akaike information criterion (AIC) to
300   determine the optimal bandwidth, and the weight outside the bandwidth was 0. AIC was a
301   standard used to measure the goodness of statistical model fit, which was based on the concept of
302   entropy and provided a standard to weigh the complexity of estimation model and the goodness
303   of fitting data. In general, when AIC was minimum, bandwidth h was the best. The expression
304   formula is as follows:

305
$$AIC = 2k - 2ln(L), \qquad (9)$$

306   where k is the number of model parameters and represents the complexity of the model; and L is
307   the likelihood function, which can reflect the degree of difference between different models.

308   **3 Results**

309   **3.1 Spatial information characteristics of landscape pattern and surface temperature**

310   ForLS, FarmLS, and ArtLS were the main landscapes of the Beijing-Tianjin-Hebei urban
311   agglomeration (Table 3). Among them, ForLS was distributed primarily in hills, FarmLS was
312   distributed mainly in the plains, and ArtLS was distributed mainly in Beijing, Tianjin,
313   Shijiazhuang, and other plain cities, accounting for 32.83%, 43.45%, and 11.96% of the total
314   area, respectively (Figure 4). Plains and hills were the main terrains in the Beijing-Tianjin-Hebei
315   region, and the plateau was small. In the plains, FarmLS and ArtLS were the primary landscape.
316   The area ratio of both reached 90%; in hills; ForLS, FarmLS, and GraLS were the main
317   landscapes, with area ratios of 59.46%, 22.48%, and 11.91%, respectively. On the plateau, the
318   landscape was dominated by FarmLS and GraLS, with an area ratio of 48.77% and 35.60%,
319   respectively.
320   Hot spots of surface temperature were distributed mainly in the southwest of the plains, the
321   southeast of the hills, and the cities like Beijing, Tianjin, Shijiazhuang; cold spots are distributed
322   mainly in the northern hills and in Yanshan and Taihang mountains (Figure 5). In the Beijing-
323   Tianjin-Hebei urban agglomeration, FarmLS and ArtLS were the main landscapes of the hot
324   spots, accounting for 62.03% and 25.70% of the total area of the hot spots, respectively. The cold
325   spots were dominated by ForLS, accounting for 78.12% of the total cold spot area. In the plains,
326   hot spots were dominated by FarmLS and ArtLS, whereas cold spots were dominated by FarmLS
327   and WetLS. In hills, hot spots were dominated by FarmLS, GraLS, and ArtLS, whereas cold
328   spots were dominated by ForLS. On the plateau, hot spots were dominated by GraLS and
329   FarmLS, whereas cold spots were dominated by GraLS, ForLS, and FarmLS.
330

331   Figure.4 Spatial distribution of landscape   Figure.5 Hot-spot analysis of surface temperature
332   Table.3 Area ratio of different landscapes

3.2 Relationship between landscape pattern and surface temperature based on different

334   **analytical window granularity**

335   The experiment showed that as window granularity increased gradually (Figure 6), the r^2 of
336   different landscape fluctuated up and down, but the fluctuation range was small. The window
337   granularity of 5 km × 5 km was the turning point at which the r^2 of ForLS, EcoLSP, and
338   GreenLSP transitioned from weak to strong and the r^2 of the other landscapes was relatively
339   strong. As window granularity increased gradually, the r^2 of FarmLS and ArtLS increased
340   gradually. Moreover, if the analysis granularity is too large, the amount of data will be reduced,
341   thus affecting the accuracy of the experiment. so the optimal analytical window granularity was
342   5 km × 5 km.
343   Figure.6 The square of Pearson correlation coefficient (r^2) based on different analytical window
344   granularity

3.3 Interpretative ability of landscape pattern to explain surface temperature

346   **3.3.1 Interpretative ability of landscape pattern to explain surface temperature in the study**

347   **area**

348   According to Table 4, we found that the interpretative ability of ForLS, FarmLS, ArtLS,
349   GreenLSP, and EcoLSP to explain surface temperature was strong, whereas the interpretative
350   ability of GraLS and WetLS to explain surface temperature was weaker. The area ratio of ForLS
351   and EcoLSP increased by 10%, the surface temperature dropped by 0.69°C and 0.63°C
352   respectively; the NDVI value increased by 0.1 which could represent GreenLSP, the surface
353   temperature dropped by 1.45°C. The area ratio of ArtLS and FarmLS increased by 10%, and the
354   surface temperature increased by 1.26°C and 0.65°C respectively, which indicated that ArtLS
355   and FarmLS was the main thermal landscape, moreover, the influence of ArtLS on surface
356   temperature is twice as great as that of FarmLS.
357
358   Table.4 Analysis results of landscape's ability to interpret surface temperature in the whole
359   domain

3.3.2 Interpretative ability of landscape pattern to explain surface temperature in different terrains

The interpretative ability of ForLS, FarmLS, ArtLS, GraLS, and EcoLSP was stronger in hills (Table 5); the interpretative ability of the GreenLSP was stronger in hills and the plateau; and the interpretative ability of WetLS was stronger in the plain.

The area ratio of ForLS and EcoLSP increased by 10% and the surface temperature dropped by 0.64°C and 0.63°C in the hills and dropped by 0.45°C and 0.41°C in the plains and dropped by 0.99°C and 0.18°C in the plateau respectively. The NDVI value increased by 0.1, the surface temperature dropped by 2.21°C in the hills, whereas the surface temperature dropped by 0.10°C in the plains. It was obvious that the cooling effect of the ForLS, EcoLSP and GreenLSP in the hills was more significant.

ArtLS and FarmLS were the main thermal landscapes. The area ratio of the ArtLS increased by 10%, the surface temperature rose by 1.69°C in the hills and increased by 0.32°C and 0.17°C respectively in the plateau and plain region. The area ratio of FarmLS increased by 10%, the surface temperature rose by 0.67°C in the hills and rose by 0.59°C and 0.12°C respectively in the plateau and plains. The degree of influence of ArtLS and FarmLS was more significant in the hills.

Although the interpretative ability of GraLS and WetLS to explain surface temperature was not strong in the Beijing-Tianjin-Hebei urban agglomeration, the relationship among GraLS, WetLS and surface temperature was significantly positive in the hills and the plateau, whereas it was significantly negative in the plains.

Table.5 Analysis results of landscape's ability to interpret surface temperature after zoning

3.3.3 Interpretative ability of landscape pattern to explain surface temperature using the GWR model

In the large-scale area of the Beijing-Tianjin-Hebei urban agglomeration, the area of GraLS and WetLS was small, and the relationship between GraLS, WetLS and surface temperature was not obvious. Therefore, we studied only the interpretative ability of the ArtLS, FarmLS, GreenLSP, and EcoLSP to explain surface temperature and we divided the research results into five grades according to the quantile method (Figure 7).

On the whole, EcoLSP and GreenLSP had a significant cooling effect. Increasing the area of ArtLS and FarmLS could promote the increase in surface temperature (Tables 6 and 7), which was consistent with the results given in Tables 4 and 5. Spatial heterogeneity was evident, however, in the interpretative ability and degree of influence of the four landscapes on surface temperature.

In hills, the class IV and V of EcoLSP R^2 values accounted for 76.13% and 62.03% of the

396   terrain, respectively, and the class IV and V coefficients accounted for 61.32% and 78.85%,
397   respectively (Table 7). This indicated that the interpretative ability and cooling ability of EcoLSP
398   to explain surface temperature were greater in hills than in the plains and the plateau, and the
399   interpretative ability was stronger at the border of the plains and hills, such as in the Yanshan and
400   Taihang mountains (Figure 7).

401   In hills, the class IV and V of GreenLSP R^2 values accounted for 75.25% and 83.82% of the
402   terrain, respectively, and the class I and II coefficients accounted for 88.29% and 87.17% of the
403   terrain, respectively (Table 7). The class V of GreenLSP R^2 was concentrated in the central hills,
404   including the Yanshan Mountains. This coefficient showed a trend of gradual decrease from the
405   southeast to the northwest in space (Figure 7), which indicated that GreenLSP had a stronger
406   interpretative power and a greater degree of influence on the surface temperature in the hills.

407   In hills, the class IV and V of FarmLS R^2 values accounted for 64.74% and 74.81% of the
408   terrain, respectively, and the class IV and V coefficients accounted for 86.40% and 92.69% of
409   the terrain, respectively (Table 7). These results showed that the interpretative ability and degree
410   of influence of FarmLS on surface temperature in the hills was stronger. In hills, the class IV and
411   V of ArtLS R^2 values accounted for 64.26% and 43.52% of the terrain, respectively. The
412   percentage of the class V of ArtLS R^2 values in the plains was 56.20% and was focused on the
413   surrounding areas of Beijing, Tianjin, and other cities, as well as on the junction of the hills and
414   plains. In hills, the class IV and V coefficients accounted for 85.10% and 92.56% of the terrain,
415   respectively (Table 7). This result showed that the interpretative ability of ArtLS to explain
416   surface temperature was stronger in the hills and the plains, and the degree of influence of ArtLS
417   on surface temperature was greater in the hills.

418

419   Table.6 GWR results of the relationship between landscape pattern and surface temperature
420   Table.7 Relationship between regression coefficient and R^2 classification in different terrains
421   Figure.7 Results of the relationship between landscape pattern and surface temperature (R^2 and
422   regression coefficient) using GWR: (A) EcoLSP and (B) GreenLSP and (C) FarmLS and (D)
423   ArtLS.

4 Discussion

4.1 The distribution of hot spots

426   In this study, the distribution of hot spots obtained using the improved hot-spot analysis
427   method was consistent with that obtained by the traditional method as a whole. In the areas with
428   high topographic relief, we find slight differences, which was consistent with the expected
429   results of the study. Therefore, if you want to study the aggregation of surface temperature or
430   other attributes in a mountain city, or an urban agglomeration with a large difference in altitude,
431   the improved three-dimensional hot-spot analysis method will theoretically more accurately
432   reflect the clustering results of the study and be more in line with real life.

433   In the distribution of hot spots, other than the hot spots in Beijing and Tianjin, large hot
434   spots appeared in Shijiazhuang, Handan, Xingtai, and Cangzhou, where the temperature was also
435   high according to the statistical yearbook for the same year as the study. Therefore, we deemed
436   the result to be accurate. The higher surface temperature in Cangzhou was closely related to the
437   development of industry, the higher surface temperature in Beijing and Tianjin was related not
438   only to the high intensity of urbanization but also to the large population and large human-made
439   heat emission. In other cities, the dimension was low, the landscape was dominated by FarmLS
440   and ArtLS, the area of EcoLSP was small, the industrial development intensity was high, the
441   artificial heat emission was relatively high, and the air pollution was serious, which was not
442   conducive to heat diffusion. The region is northwest of the Taihang mountains and the slope was
443   mostly from east to south (Jiao et al., 2019).

4.2 Exploration of optimal analytical window granularity

445   On the basis of the 1000-meter-resolution land surface temperature data, we concluded that
446   the optimal analytical window granularity for the expression of the relationship between
447   landscape pattern and surface temperature was 5 km × 5 km in the Beijing-Tianjin-Hebei urban
448   agglomeration. On the basis of the 30-meter-resolution surface temperature data, Guo et al.
449   (2012) concluded that the optimal analytical window of the relationship between landscape
450   pattern and surface temperature in the Pearl River Delta in China was 150 m × 150 m.
451   Conversely, Weng et al. (2007) concluded that the optimal analytical window of the relationship
452   between landscape pattern and surface temperature in Indianapolis, United States, was 120 m ×
453   120 m. Lu et al. (2018) used 120-meter-resolution surface temperature data and found that the
454   granularity of the analytical window of 1.8 km × 1.8 km was optimal in Hangzhou, China. This
455   indicated that the granularity of the optimal analytical window for the expression of the
456   relationship between landscape pattern and surface temperature was related not only to regional
457   location and regional scale differences but also to the resolution of surface temperature and
458   landscape pattern data sources.

4.3 Interpretative ability of landscape pattern to explain surface temperature

460   In the Beijing-Tianjin-Hebei region, the interpretative ability of GraLS and WetLS to
461   explain surface temperature was weak and inconsistent in different terrains. This phenomenon is
462   not consistent with life experience and the results of Kumar et al. (2015), Zhi et al. (2013).
463   However, the study by Yi et al. (2018) found that the relationship between WetLS and surface
464   temperature was unstable and possibly positively correlated comparing the relationship between
465   WetLS and surface temperature in Jinan and Chongqing. Meanwhile, Xiao et al. (2018)
466   compared the relationship among large GreenLSP, small GreenLSP, and surface temperature.
467   They found that the cooling effect of large GreenLSP was more apparent and more stable,
468   whereas the cooling effect of small GreenLSP was not obvious and was not stable. This finding

469   indicated that in unit area, if the area percentage of a landscape was small, the relationship
470   between the landscape pattern and surface temperature was unstable. In the Beijing-Tianjin-
471   Hebei region, because WetLS is small and scattered, we should protect the Baiyangdian, Yuqiao
472   reservoir and other wetland, maintain the flow of the river, and prevent the phenomenon of
473   interruption. The area percentage of ForLS and EcoLSP increased by 10%, and the surface
474   temperature dropped by 0.69°C and 0.63°C, respectively, indicating that the cooling capacity of
475   EcoLSP, GraLS, and WetLS was lower than that of ForLS alone. It showed that the cooling
476   capacity of GraLS and WetLS was less than that of ForLS and either one of the two was less
477   than the cooling capacity of ForLS. According to the study by Zhi et al. (2013), the cooling
478   capacity of GraLS was smaller than that of ForLS because the thermal inertia of GraLS was
479   smaller than that of ForLS, whereas the WetLS had a larger thermal inertia, and its cooling
480   capacity was larger than that of ForLS. In fact, in the Beijing-Tianjin-Hebei region, a large area
481   of WetLS concentrated in the low-altitude region of the Bohai Rim, the regional urbanization
482   level was higher, the population was concentrated, industry had developed, and the sea land
483   building and other human activities were evident, which all contributed to higher surface
484   temperatures in the surrounding WetLS. ForLS, however, was distributed mainly in hilly regions
485   with less human activities and a higher altitude, so it was reasonable to assume that the cooling
486   effect of WetLS was less significant than that of ForLS. The NDVI value increased by 0.1 and
487   the surface temperature dropped by 1.45°C. This result indicated that the GreenLSP cooling
488   effect was obvious, which was consistent with the research results of Li et al. (2018), Zhang et al.
489   (2009), Chen et al. (2006) and Huang et al. (2018). GreenLSP not only can generate shadows and
490   increase air humidity through transpiration (Taha, 1997; De Munck et al., 2017) but it also can
491   increase surface roughness and improve the efficiency of air convection (Gunawardena et al.,
492   2017) to achieve the purpose of cooling. The influence of ArtLS on surface temperature was
493   twice as great as that of FarmLS, and this phenomenon mainly related to the surface reflectance
494   and the human activities (Zhi et al., 2013).
495   Studies have shown that in regions with complex mountain environmental conditions,
496   elevation, slope, slope direction, and other key topographic factors have a significant impact on
497   surface temperature (Jiao et al., 2019). The interpretation and cooling capacity of EcoLSP on
498   surface temperature in hilly areas was greater than that in the plains and the plateau. In hilly
499   areas, the proportion of EcoLSP area was more than 70% (Table 3), the connectivity was strong,
500   and the human disturbance was insignificant, and thus it had a strong cooling capacity. In the
501   plains, the area percentage of EcoLSP was less than 10% (Table 3), the degree of EcoLSP
502   fragmentation was high, the area percentage of ArtLS was large, the population was concentrated,
503   and the artificial heat emission was large. The urban environmental stress made the forest
504   vegetation growth worse, resulting in weak vegetation transpiration (Philip et al., 2005). In the
505   plateau area, although the area percentage of EcoLSP was 44.20%, GraLS was the main EcoLSP,
506   which had a smaller cooling capacity than ForLS, and the area percentage of FarmLS was
507   48.77%. Therefore, the cooling capacity of EcoLSP in the plateau area was significantly lower
508   than that in the hilly area. The interpretative ability and degree of influence of GreenLSP on
509   surface temperature were stronger and larger in hilly areas. Although the NDVI value in the

510 plains and the plateau was larger, the landscape in this region was predominately FarmLS (dry
511 land) and ArtLS, both of which were thermal landscapes with higher surface temperatures. In
512 hilly areas, which were in the northwestern study area, ForLS and GraLS were the primary
513 landscapes, both non-thermal landscape, the altitude was higher, and the thermal inertia of
514 FarmLS was significantly smaller than that of ForLS (Zhi et al., 2013). The interpretative ability
515 and degree of influence of FarmLS and ArtLS on surface temperature were stronger and greater
516 in hilly areas. The main landscapes in hilly areas were EcoLSP and ForLS. If the area of ArtLS
517 and FarmLS increased, which occupied the original EcoLSP, the EcoLSP area decreased. In
518 addition, a lot of human activity not only increased the fragmentation of EcoLSP but also
519 introduced environmental disturbances that could affect the growth of the surrounding forest and
520 cooling capacity to reduce the cooling ability of EcoLSP(Jones et al., 1990; Shen et al., 2015).
521   However, we analyzed only the interpretative ability of landscape pattern to explain surface
522 temperature from the perspective of an urban agglomeration scale. It did not conduct relevant
523 research from the perspective of different urban areas and compare them. Therefore, a
524 comparative analysis of differences in interpretative ability between the urban agglomeration
525 scale and the city scale should be the primary focus of follow-up research. In the process of an
526 interpretative ability analysis, to avoid the multicollinearity problem among landscape
527 proportions, we adopted single-factor regression analysis. In the follow-up study, multifactor
528 regression analysis could be considered to explore the interpretative ability of different
529 landscapes to explain surface temperature.

5 Conclusions

531   In this study, we quantitatively analyzed the spatial pattern characteristics of surface
532 temperature and landscape using an improved three-dimensional hot-spot analysis method. With
533 the help of a Pearson correlation coefficient, OLS, and GWR model, we explored the optimal
534 analytical window granularity of the relationship between landscape pattern and surface
535 temperature, and we discussed the spatial heterogeneity of the degree of influence and the
536 interpretative ability of four landscapes on surface temperature. The main conclusions follow.
537 (1) The improved three-dimensional hot-spot analysis method is more suitable for the spatial
538 heterogeneity analysis of surface temperature in some mountainous cities or urban
539 agglomerations with complex topography and large difference in altitude, and the results
540 obtained are more in line with the real life scene in concept than the traditional two-dimensional
541 hot-spot analysis method.
542 (2) Under an analytical window granularity of 5 km × 5 km, the Pearson correlation coefficient
543 between ForLS, EcoLSP, GreenLSP and surface temperature in the Beijing-Tianjin-Hebei urban
544 agglomeration was larger than that obtained using other analytical window granularity values.
545 (3) In the Beijing-Tianjin-Hebei region, the hot spots of surface temperature were distributed
546 mainly in the southwestern plain, southeastern hills, Beijing, Tianjin, Shijiazhuang, and other
547 urban areas, primarily those with ArtLS and FarmLS. The cold spots were distributed mainly in
548 the northern hills and the Yanshan and Taihang mountains.

549   ForLS, FarmLS, ArtLS, GreenLSP, and EcoLSP had a strong ability to explain surface
550   temperature, whereas GraLS and WetLS had a weak ability to explain surface temperature.
551   There was spatial heterogeneity in the interpretative ability of EcoLSP, GreenLSP, ArtLS and
552   FarmLS to explain surface temperature. The interpretative ability and the thermal control ability
553   of these four landscapes were more significant in the hills than in the plains and the plateau. The
554   interpretative ability of EcoLSP to explain surface temperature was stronger at the junction of the
555   plains and hills, especially in the Yanshan and Taihang mountains. The interpretative ability of
556   ArtLS was stronger in the areas surrounding of cities, including Beijing and Tianjin, and at the
557   junction of the plains and hills.

558   Therefore, under the background of coordinated and integrated development in the Beijing-
559   Tianjin-Hebei urban agglomeration, to avoid a highly fragmented landscape, urban construction
560   should be rationally distributed. The area of EcoLSP, ForLS within and between cities should be
561   increased, especially around Beijing and Tianjin, and the level of development in the Yanshan
562   and Taihang mountains and other areas dominated by natural landscape should be reduced.
563   Doing so will promote the sustainable development of the Beijing-Tianjin-Hebei region.

564

565 Acknowledgments

566   This research was funded by the Major Project of the National Natural Science Foundation
567   of China (No. 41590841), the National Key Research and Development Plan (No.
568   2016YFC0503001), the Natural Science Foundation of Tianjin, China (No. 18JCYBJC90900),
569   and the Project of Scientific Research Plan of Tianjin Education Commission (No. 2018KJ164)
570   and Tianjin Education Commission Research Project (No. 2016CJ20).

571   D.W. and Z.S. conceived and designed the research; D.W. and Z.S. performed the
572   experiments; J.C. and Z.S. drafted the article; J.C., Z.S., X.Z., X.W., and W.Z. collected and
573   processed the data; J.C., X.Z., and Z.S. analyzed the data; D.W. and Z.S. discussed and modified
574   the original manuscript; and D.W. and Z.S. polished the language of the paper. All of the authors
575   revised the article critically and approved the final manuscript. RS data were downloaded from
576   the Geographic Spatial Data Cloud. The authors would like to thank everyone who contributed to
577   the study and research. We thank Accdon (www.accdon.com) for its linguistic assistance during
578   the preparation of this manuscript. Remote-sensing data were downloaded from the Geographic
579   Spatial Data Cloud and EARTHDATA Search.

580 References

581   Amiri R, Weng Q-H, Alimohammadi A, Alavipanah SK. 2009. Spatial–temporal dynamics of
582   land surface temperature in relation to fractional vegetation cover and land cover/cover in the
583   Tabriz urban area, Iran. Remote Sensing of Environment 113(12):2606-2617 DOI
584   10.1016/j.rse.2009.07.021.

585 Angel S, Parent J, Civco DL, Blei A, Potere D. 2011. The dimensions of global urban expansion:
586 Estimates and projections for all countries, 2000–2050. Progress in Planning 75(2):53-107 DOI
587 10.1016/j.progress.2011.04.001.
588 Asgarian A, Amiri BJ, Sakieh Y. 2015. Assessing the effect of green cover spatial patterns on
589 urban land surface temperature using landscape metrics approach. Urban Ecosystems 18(1):209-
590 222 DOI 10.1007/s11252-014-0387-7.
591 Barrington-Leigh C, Millard-Ball A. 2015. A century of sprawl in the United States. Proceedings
592 of the National Academy of Sciences 112(27):8244-8249 DOI 10.1073/pnas.1504033112.
593 Bonafoni, S, Baldinelli, G, Verducci, P, Presciutti, A, 2017. Remote sensing techniques for urban
594 heating analysis: a case study of sustainable construction at district level. Sustainability 9:1308
595 DOI 10.3390/su9081308.
596 Chen AL, Sun RH, Chen LD. 2012. Studies on urban heat island from a landscape pattern view:
597 a review. Acta Ecologica Sinica 32(14):4553-4565 [in Chinese].
598 Chen J, Wang CZ, Jiang H, Miao LX, Yu ZR. 2011. Estimating soil moisture using
599 Temperature–Vegetation Dryness Index (TVDI) in the Huang-huai-hai (HHH) plain.
600 International Journal of Remote Sensing 32(4):1165-1177 DOI 10.1080/01431160903527421
601 Chen XL, Zhao HM, Li PX, Yin J. 2006. Remote sensing image-based analysis of the
602 relationship between urban heat island and land cover/cover changes. Remote Sensing of
603 Environment 104(2):133-146 DOI 10.1016/j.rse.2005.11.016.
604 Connors JP, Galletti CS, Chow WTL. 2013. Landscape configuration and urban heat island
605 effects: assessing the relationship between landscape characteristics and land surface temperature
606 in Phoenix, Arizona. Landscape Ecology 28(2): 271-283 DOI 10.1007/s10980-012-9833-1
607 De Munck C, Lemonsu A, Masson V, Le Bras J, Bonhomme M. 2018. Evaluating the impacts of
608 greening scenarios on thermal comfort and energy and water consumptions for adapting Paris
609 city to climate change. Urban Climate 23:260–286 DOI 10.1016/j.uclim.2017.01.003.
610 Du HY, Wang DD, Wang YY, Zhao XL, Qin F, Jiang H, Cai Y-L. 2016. Influences of land
611 cover types, meteorological conditions, anthropogenic heat and urban area on surface urban heat
612 island in the Yangtze River Delta Urban Agglomeration. Science of The Total Environment, 571:
613 461-470 DOI 10.1016/j.scitotenv.2016.07.012.
614 Duan XW, Zhang GL, Rong L, Fang HY, He DM, Feng DT. 2015. Spatial distribution and
615 environmental factors of catchment-scale soil heavy metal contamination in the dry-hot valley of
616 Upper Red River in southwestern China. Catena (135):59–69 DOI 10.1016/j.catena.2015.07.006.
617 Estoque RC, Murayama Y, Myint SW. 2017. Effects of landscape composition and pattern on
618 land surface temperature: An urban heat island study in the megacities of Southeast Asia.
619 Science of the Total Environment 577:349-359 DOI 10.1016/j.scitotenv.2016.10.195.
620 Farahani HA, Rahiminezhad A, Same L, Immannezhad K, . 2010. A Comparison of Partial Least
621 Squares (PLS) and Ordinary Least Squares (OLS) regressions in predicting of couples mental
622 health based on their communicational patterns. Procedia-Social and Behavioral Sciences 5:
623 1459-1463 DOI 10.1016/j.sbspro.2010.07.308.
624 Feng YJ, Chen XJ, Feng G, Liu Y. 2018. Impacts of changing scale on Getis-Ord Gi* hotspots of
625 CPUE: a case study of the neon flying squid (Ommastrephes bartramii) in the northwest Pacific

626   Ocean. Acta Oceanologica Sinica 37(5):67-76 DOI CNKI:SUN:SEAE.0.2018-05-009.

627   Ferreira LG, Sano EE, Fernandez LE, Araújo FM. 2013. Biophysical characteristics and fire
628   occurrence of cultivated pastures in the Brazilian savanna observed by moderate resolution
629   satellite   data.   International   Journal   of   Remote   Sensing   34(1):154-167   DOI
630   10.1080/01431161.2012.712223

631   Gage EA, Cooper DJ. 2017. Relationships between landscape pattern metrics, vertical structure
632   and surface urban Heat Island formation in a Colorado suburb. Urban Ecosystems 20(6):1-10
633   DOI 10.1007/s11252-017-0675-0.

634   Gu ZJ, Duan XW, Liu B, Hu JM, He JN. 2016. The spatial distribution and temporal variation of
635   rainfall erosivity in the Yunnan Plateau, Southwest China: 1960–2012. CATENA 145:291-300
636   DOI 10.1016/j.catena.2016.06.028.

637   Gunawardena KR, Wells MJ, Kershaw T. 2017. Utilising green and bluespace to mitigate urban
638   heat   island   intensity.   Science   of   The   Total   Environment   584:1040-1055   DOI
639   10.1016/j.scitotenv.2017.01.158.

640   Guo GH, Chen YB, Wei JB, Wu ZF, Rong XZ. 2012. Impacts of grid sizes on urban heat island
641   pattern analysis. Acta Ecologica Sinica 32(12): 3764-3772 [in Chinese].

642   Guo L, Ma ZH, Zhang LJ. 2008. Comparison of bandwidth selection in application of
643   geographically   weighted   regression: a   case   study.   Canadian   Journal   of   Forest   Research
644   38(9):2526-2534 DOI 10.1139/X08-091.

645   Huang M, Cui P, He X. 2018. Study of the cooling effects of urban green space in Harbin in
646   terms of reducing the heat island effect. Sustainability 10:1101 DOI 10.3390/su10041101.

647   Jiao ZH, Yan GJ, Wang TX, Mu XH, Zhao J. 2019. Modeling of Land Surface Thermal
648   Anisotropy Based on Directional and Equivalent Brightness Temperatures Over Complex
649   Terrain. IEEE Journal of Selected Topics in Applied Earth Observations and Remote Sensing,
650   12(2):410-423 DOI 10.1109/JSTARS.2018.2855192.

651   Jones PD, Groisman PY, Coughlan M, Plummer N, Wang W-C, Karl TR. 1990. Assessment of
652   urbanization effects in time series of surface air temperature over land. Nature 347(6289):169-
653   172 DOI 10.1038/347169a0.

654   Kumar D, Shekhar S. 2015. Statistical analysis of land surface temperature–vegetation indexes
655   relationship through thermal remote sensing. Ecotoxicology and Environmental Safety 121:39-
656   44 DOI 10.1016/j.ecoenv.2015.07.004.

657   Li B, Liu ZF, Nan Y, Li SN, Yang YM. 2018. Comparative Analysis of Urban Heat Island
658   Intensities   in   Chinese,   Russian,   and   DPRK   Regionsacross   the   Transnational   Urban
659   Agglomeration   of   the   Tumen   River   in   Northeast   Asia.   Sustainability   10:2637   DOI
660   10.3390/su10082637.

661   Li J, Zhang Y, Wang X, Qin QM, Wei ZZ, Li JZ., 2016. Application of GPS Trajectory Data for
662   Investigating the Interaction between Human Activity and Landscape Pattern: A Case Study of
663   the Lijiang River Basin, China. ISPRS International Journal of Geo-Information 5(7):104 DOI
664   10.3390/ijgi5070104.

665   Li JX, Song CH, Cao L, Zhu FG, Meng XL, Wu JG. 2011. Impacts of landscape structure on
666   surface urban heat islands: a case study of Shanghai, China. Remote Sensing of Environment

667 115(12):3249-3263 DOI 10.1016/j.rse.2011.07.008.

668 Li MM, Wang TJ, Xie M, Zhuang BL, Li S, Han Y, Cheng BL, . 2017. Modeling of urban heat
669 island and its impacts on thermal circulations in the Beijing–Tianjin–Hebei region, China.
670 Theoretical and Applied Climatology 128(3-4):999-1013 DOI 10.1007/s00704-016-1903-x.

671 Li SC, Zhao ZQ, Xie MM, Wang YL. 2010. Investigating spatial non-stationary and scale-
672 dependent relationships between urban surface temperature and environmental factors using
673 geographically weighted regression. Environmental Modelling & Software 25(12):1789-1800
674 DOI 10.1016/j.envsoft.2010.06.011.

675 Li WF, Cao QW, Lang K, Wu JS. 2017. Linking potential heat source and sink to urban heat
676 island: heterogeneous effects of landscape pattern on land surface temperature. Science of the
677 Total Environment 586:457-465 DOI 10.1016/j.scitotenv.2017.01.191.

678 Lu HM, Li F, Zhang ML, Yang G, Sun WW. 2018. Effects of landscape pattern on annual
679 variation of thermal environment in Hangzhou. Remote Sensing Technology and Application
680 3:398-407 [in Chinese].

681 Miao CY, Ashouri H, Hsu K, Sorooshian S, Duan QY. 2015. Evaluation of the PERSIANN-
682 CDR daily rainfall estimates in capturing the behavior of extreme precipitation events over
683 China. Journal of Hydrometeorology 16:1387–1396 DOI 10.1175/JHM-D-14-0174.1.

684 Miao CY, Ni JR, Borthwick AGL, Yang L, . 2011. A preliminary estimate of human and natural
685 contributions to the changes in water discharge and sediment load in the Yellow River. Global
686 and Planetary Change 76(3-4): 196-205 DOI 10.1016/j.gloplacha.2011.01.008.

687 Miao CY, Ni JR. Borthwick AGL. 2010. Recent changes of water discharge and sediment load
688 in the Yellow River basin, China. Progress in Physical Geography 34(4):541-561 DOI
689 10.1177/0309133310369434.

690 Philip E, Azlin YN. 2005. Measurement of soil compaction tolerance of Lagestromia speciosa
691 (L.) Pers. using chlorophyll fluorescence. Urban Forestry and Urban Greening 3(3):203-208 DOI
692 10.1016/j.ufug.2005.04.003.

693 Shen GR, Ibrahim AN, Wang ZJ, Ma C, Gong JH. 2015. Spatial–temporal land-use/land-cover
694 dynamics and their impacts on surface temperature in Chongming Island of Shanghai, China.
695 International Journal of Remote Sensing 36(15):4037-4053 DOI
696 10.1080/01431161.2015.1043404.

697 Su SL, Xiao R, Jiang ZL, Zhang Y. 2012. Characterizing landscape pattern and ecosystem
698 service value changes for urbanization impacts at an eco-regional scale. Applied Geography
699 34(1):295-305 DOI 10.1016/j.apgeog.2011.12.001.

700 Taha H. 1997. Urban climates and heat islands: albedo, evapotranspiration, and anthropogenic
701 heat. Energy and Buildings 25(2):99-103 DOI 10.1016/S0378-7788(96)00999-1.

702 Wang HT, Zhang YZ, Tsou JY, Li Y. 2017. Surface Urban Heat Island Analysis of Shanghai
703 (China) Based on the Change of Land cover and Land Cover. Sustainability 9:1538 DOI
704 10.3390/su9091538.

705 Weng QH, Liu H, Lu DS. 2007. Assessing the effects of land cover and land cover patterns on
706 thermal conditions using landscape metrics in city of Indianapolis,, United States.. Urban
707 Ecosystems 10(2): 203-219 DOI 10.1007/s11252-007-0020-0..

708 Xiao HL, Weng QH. 2007. The impact of land cover and land cover changes on land surface
709 temperature in a karst area of China. Journal of Environmental Management 85(1):245-257 DOI
710 10.1016/j.jenvman.2006.07.016.
711 Xiao XD, Dong L, Yan HN, Yang N, Xiong Y-M. 2018. The influence of the spatial
712 characteristics of urban green space on the urban heat island effect in Suzhou Industrial Park.
713 Sustainable Cities and Society 40:428-439 DOI 10.1016/j.scs.2018.04.002.
714 Yi CX, Hu JC, Li XJ. 2018. Response analysis of land cover types on urban heat island effect.
715 Bulletin of Surveying and Mapping (1):72-76 [in Chinese].
716 Zhang D, Huang QX, He CY, Wu JG. 2017. Impacts of urban expansion on ecosystem services
717 in the Beijing-Tianjin-Hebei urban agglomeration, China: A scenario analysis based on the
718 Shared Socioeconomic Pathways. Resources Conservation and Recycling 125:115-130 DOI
719 10.1016/j.resconrec.2017.06.003.
720 Zhang XY, Zhong TY, Feng XZ, Wang K. 2009. Estimation of the relationship between
721 vegetation patches and urban land surface temperature with remote sensing. International Journal
722 of Remote Sensing 30(8):2105-2118 DOI 10.1080/01431160802549252.
723 Zhang YS, Odeh IOA, Han CF. 2009. Bi-temporal characterization of land surface temperature
724 in relation to impervious surface area, NDVI and NDBI, using a sub-pixel image analysis.
725 Chinese Journal of Osteoporosis 11(4):256-264 DOI 10.1016/j.jag.2009.03.001.
726 Zhao CH, Jensen J, Weng QH, Weaver R. 2018. A Geographically Weighted Regression
727 Analysis of the Underlying Factors Related to the Surface Urban Heat Island Phenomenon.
728 Remote Sensing 10:1428 DOI 10.3390/rs10091428.
729 Zhao HB, Zhang H, Miao CH, Ye XY, Min M. 2018. Linking Heat Source–Sink Landscape
730 Patterns with Analysis of Urban Heat Islands: Study on the Fast-Growing Zhengzhou City in
731 Central China. Remote Sensing 10(8):1268 DOI 10.3390/rs10081268.
732 Zhi Q, Tian G, Lin X. 2013. Diurnal and seasonal impacts of urbanization on the urban thermal
733 environment: A case study of Beijing using MODIS data. Isprs Journal of Photogrammetry and
734 Remote Sensing 85(2):93-101 DOI 10.1016/j.isprsjprs.2013.08.010.
735 Zhou DC, Bonafoni S, Zhang LX, Wang RH. 2018. Remote sensing of the urban heat island
736 effect in a highly populated urban agglomeration area in East China. Science of the Total
737 Environment 628-629:415-429 DOI 10.1016/j.scitotenv.2018.02.074.
738 Zhou XL, Wang YC. 2011. Dynamics of Land Surface Temperature in Response to
739 Land‐Use/Cover Change. Geographical Research 49(1):23-36 DOI 10.1111/j.1745-
740 5871.2010.00686.x.
741 Zullo F, Fazio G, Romano B, Marucci A, Fiorini L. 2019. Effects of Urban Growth Spatial
742 Pattern (UGSP) on the Land Surface Temperature (LST): a study in the Po Valley (Italy).
743 Science of the Total Environment 650:1740-1751 DOI: 10.1016/j.scitotenv.2018.09.331.

Table 1 Data sources

State the name , source, date, type, resolution, download website of the data.

Table.1 Data sources

Name	Source	Date	Type	Resolution /m	Website
Land cover	Landsat8 OLI remote sensing image	2015.07.12, 2015.07.28	Raster	30	Geospatial data cloud (http://www.gscloud.cn/)
DEM	ASTER GDEM remote sensing image		Raster	30	
Surface temperature	MODIS surface temperature 8 days synthesis product (MOD 11A2)	2015.07.04, 2015.07.12, 2015.07.20, 2015.07.28	Raster	1000	EARTHDATA Search (https://search.earthdata.nasa. gov/search)
NDVI	MODIS vegetation index 16 days synthetic product (MOD 13A1)	2015.07.12, 2015.07.28	Raster	500	
Topographic			Vector		Geographic Information Monitoring Cloud Platform (http://www.dsac.cn/)

Table 2 Z score, p value, confidence level, and explanation

The results of hotspot analysis are illustrated, such as Z score, p value, confidence level, and explanation.

Table.2 Z score, p value, confidence level, and explanation

Z score	P	Confidence level	Explanation
$Z(G_i^*) < -1.65$	< 0.1	$> 90\%$	Significant cold spots
$-1.65 < Z(G_i^*) < 1.65$	> 0.1	$< 90\%$	Insignificant region
$Z(G_i^*) > +1.65$	< 0.1	$> 90\%$	Significant hot spots

Table 3 Area ratio of different landscapes

It shows the area ratio of different landscapes at different spatial levels.

Table.3 Area ratio of different landscapes

Region		Area ratio of landscape (%)					
		ForLS	GraLS	WetLS	FarmLS	ArtLS	BareLS
Study area	The whole area	32.83%	8.82%	2.66%	43.45%	11.96%	0.27%
	Hot spots	2.81%	7.51%	1.74%	62.03%	25.70%	0.21%
	Cold spots	78.12%	6.65%	1.51%	12.27%	1.20%	0.25%
Plains	The whole area	2.80%	0.87%	4.93%	69.44%	21.82%	0.15%
	Hot spots	1.07%	1.01%	2.04%	67.39%	28.43%	0.07%
	Cold spots	0.43%	0.99%	40.28%	51.21%	6.95%	0.14%
Hills	The whole area	59.46%	11.91%	0.92%	22.48%	5.05%	0.18%
	Hot spots	9.41%	23.87%	0.52%	48.95%	16.73%	0.51%
	Cold spots	80.99%	5.83%	0.73%	11.22%	1.09%	0.14%
Plateau	The whole area	6.21%	35.60%	2.39%	48.77%	5.08%	1.94%
	Hot spots	1.81%	52.84%	4.20%	32.49%	4.52%	4.13%
	Cold spots	30.59%	34.40%	2.52%	26.63%	2.93%	2.93%

Table 4 Analysis results of landscape's ability to interpret surface temperature in the whole domain

Analysis results of landscape's ability to interpret surface temperature in the whole domain.

Table.4 Analysis results of landscape's ability to interpret surface temperature in the whole domain

Landscape	OLS regression	R^2	r
ForLS	Y = −6.94X + 33.84	0.57	−0.76**
GraLS	Y = −0.43X + 31.58	0.00	−0.02
WetLS	Y = 0.89X + 31.52	0.00	0.03
FarmLS	Y = 6.47X + 28.76	0. 39	0.55**
ArtLS	Y = 12.60X + 30.05	0.30	0.62**
EcoLSP	Y = −6.34X + 34.41	0.56	−0.73**
GreenLSP	Y = −14.53X + 41.31	0.28	−0.53**

** There was a significant correlation at the 0.01 level (bilateral)

Table 5 Analysis results of landscape's ability to interpret surface temperature after zoning

Analysis results of landscape's ability to interpret surface temperature after zoning.

Table.5 Analysis results of landscape's ability to interpret surface temperature after zoning

Landscape	Terrain	OLS regression	R^2	r
ForLS	Plain	Y = −4.45X + 34.20	0.07	−0.27[**]
	Hills	Y = −6.44X + 33.45	0.44	−0.67[**]
	Plateau	Y = −9.97X + 32.25	0.42	−0.64[**]
GraLS	Plain	Y = −1.37X + 34.06	0.03	−0.04
	Hills	Y = 5.05X + 29.10	0.08	0.28[**]
	Plateau	Y = 2.19X + 30.54	0.04	0.19[*]
WetLS	Plain	Y = −3.87X + 34.26	0.13	−0.36[**]
	Hills	Y = 2.44X + 29.68	0.00	0.05
	Plateau	Y = 4.48X + 31.22	0.03	0.17[*]
FarmLS	Plain	Y = 1.18X + 33.29	0.02	0.30[**]
	Hills	Y = 6.72X + 28.15	0.25	0.51[**]
	Plateau	Y = 5.86X + 31.07	0.02	0.16[*]
ArtLS	Plain	Y = 3.19X + 33.35	0.09	0.16[*]
	Hills	Y = 16.87X + 28.74	0.26	0.50[**]
	Plateau	Y = 1.69X + 30.56	0.03	0.14[*]
EcoLSP	Plain	Y = −4.06X + 34.45	0.21	−0.15[*]
	Hills	Y = −6.34X + 34.21	0.34	−0.58[**]
	Plateau	Y = −1.78X + 32.22	0.03	−0.18[*]
GreenLSP	Plain	Y = −1.01X + 34.69	0.01	−0.07
	Hills	Y = −22.12X + 45.34	0.53	−0.73[**]
	Plateau	Y = −20.79X + 43.16	0.68	−0.83[**]

** There is a significant correlation at the 0.01 level (bilateral)

* There is a significant correlation at the 0.05 level (bilateral)

Table 6 GWR results of the relationship between landscape pattern and surface temperature

GWR results of the relationship between landscape pattern and surface temperature.

Table.6 GWR results of the relationship between landscape pattern and surface temperature

Landscape	GWR regression coefficient			Average R^2	Bandwidth/m
	Minimum	Maximum	Average		
EcoLSP	−77.73	10.86	−6.36	0.56	31190.35
GreenLSP	−54.98	19.61	−12.98	0.53	46513.73
FarmLS	−61.08	162.27	3.98	0.65	16327.41
ArtLS	−55.32	410.73	16.11	0.62	18669.30

Table 7 Relationship between regression coefficient and R^2 classification in different terrains

Relationship between regression coefficient and R2 classification in different terrains :

1   Table.7 Relationship between regression coefficient and R2 classification in different terrains

Landscape	Classification results	Classification standard of coefficient	Area ratio (%)			Classification standard of R^2	The area ratio (%)		
			Plain	Hills	Plateau		Plain	Hills	Plateau
EcoLSP	I	−77.73 ~ −7.35	38.38%	61.32%	0.30%	0.00 ~ 0.06	56.59%	21.91%	21.50%
	II	−7.35 ~ −5.62	20.51%	78.85%	0.64%	0.06 ~ 0.14	46.15%	48.03%	5.82%
	III	−5.62 ~ −4.24	43.77%	53.92%	2.31%	0.14 ~ 0.23	42.63%	54.69%	2.68%
	IV	−4.24 ~ −2.86	55.36%	41.36%	3.28%	0.23 ~ 0.35	23.47%	76.13%	0.40%
	V	−2.86 ~ 10.25	48.32%	27.63%	24.04%	0.35 ~ 0.77	37.97%	62.03%	0.00%
GreenLSP	I	−54.98 ~ −21.83	0.00%	88.29%	11.71%	0.00 ~ 0.05	74.25%	21.08%	4.68%
	II	−21.83 ~ −17.23	7.08%	87.17%	5.75%	0.05 ~ 0.16	62.22%	33.35%	4.43%
	III	−17.23 ~ −9.96	31.87%	59.80%	8.33%	0.16 ~ 0.29	43.14%	48.81%	8.05%
	IV	−9.96 ~ −5.32	86.61%	11.19%	2.20%	0.29 ~ 0.47	15.22%	75.25%	9.53%
	V	−5.32 ~ 19.08	81.53%	16.10%	2.37%	0.47 ~ 0.78	12.48%	83.82%	3.70%
FarmLS	I	−57.64 ~ −2.68	80.89%	5.82%	13.29%	0.00 ~ 0.03	67.88%	20.06%	12.06%
	II	−2.68~ 0.94	71.91%	18.86%	9.23%	0.03 ~ 0.10	47.29%	44.85%	7.85%
	III	0.94 ~ 4.55	36.15%	59.37%	4.48%	0.10 ~ 0.20	35.52%	59.27%	5.21%
	IV	4.55 ~ 8.17	11.22%	86.40%	2.38%	0.20 ~ 0.32	31.64%	64.74%	3.61%
	V	8.17 ~ 126.05	6.26%	92.69%	1.05%	0.32 ~ 0.83	24.45%	73.81%	1.74%
ArtLS	I	−53.87 ~ 1.70	65.19%	18.46%	16.36%	0.00 ~ 0.05	47.54%	30.37%	22.08%
	II	1.70 ~ 5.07	81.64%	16.18%	2.19%	0.05 ~ 0.12	38.52%	56.21%	5.27%
	III	5.07 ~ 11.81	45.06%	51.63%	3.31%	0.12 ~ 0.19	29.20%	68.41%	2.39%
	IV	11.81 ~ 25.28	10.67%	85.10%	4.22%	0.19 ~ 0.29	34.99%	64.26%	0.75%
	V	25.28 ~ 373.87	3.05%	92.56%	4.39%	0.29 ~ 0.82	56.20%	43.52%	0.29%

Figure 1

Figure 1 Location of the Beijing-Tianjin-Hebei urban agglomeration

In the figure 1, the blue areas represent the administrative areas of China, and the pink areas represent the administrative areas of the Beijing-Tianjin-Hebei urban agglomeration. A hillshaded relief (Azimuth: 315, Altitude: 45, the effect was the position of the sun in the afternoon of Beijing winter, and the transparency of this layer was 30% when the map was created) was superimposed with Elevation in the right figure.
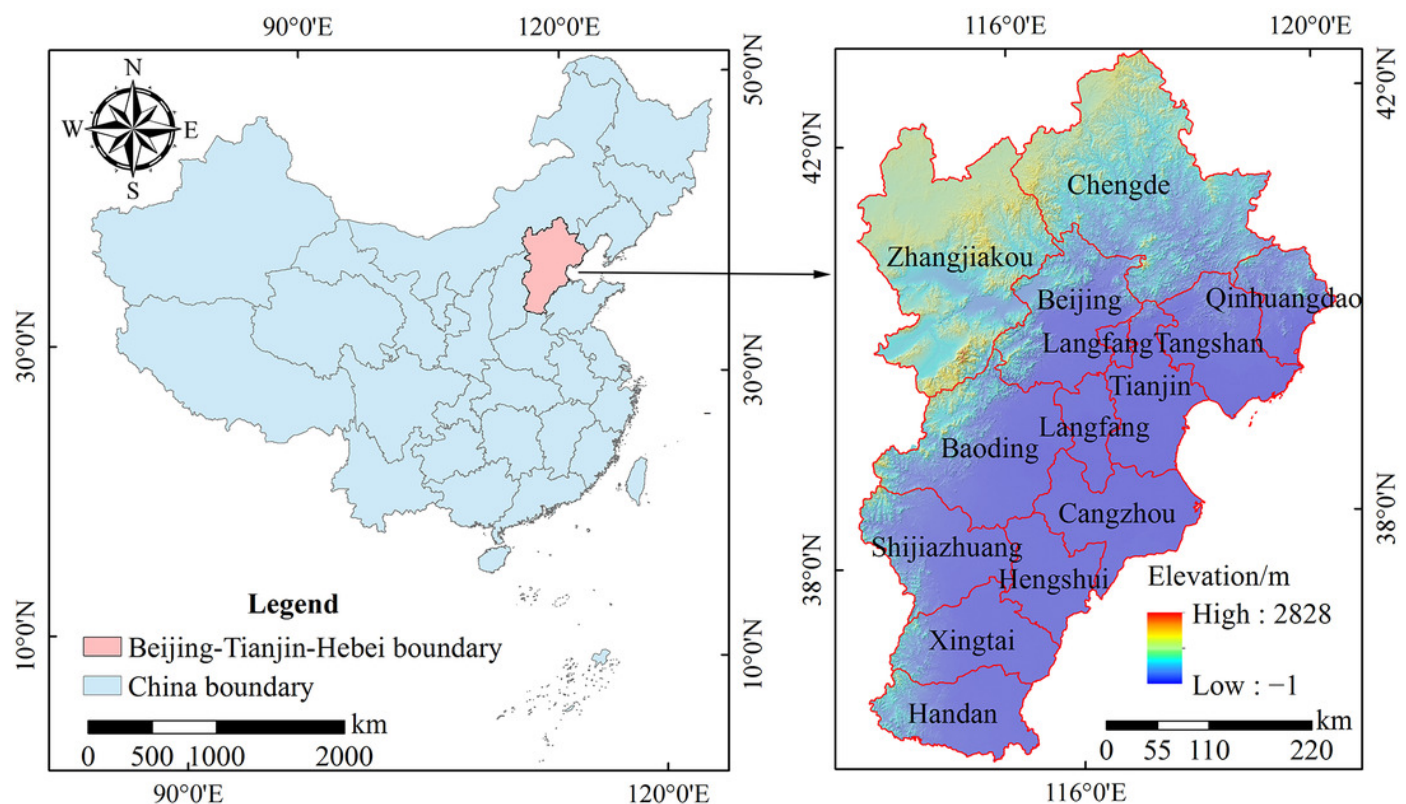
Figure 2

Figure.2 The flowchart of the paper structure

Figure.2 mainly expresses the flow chart of this study, which includes the main data, main content and main research methods of this study.
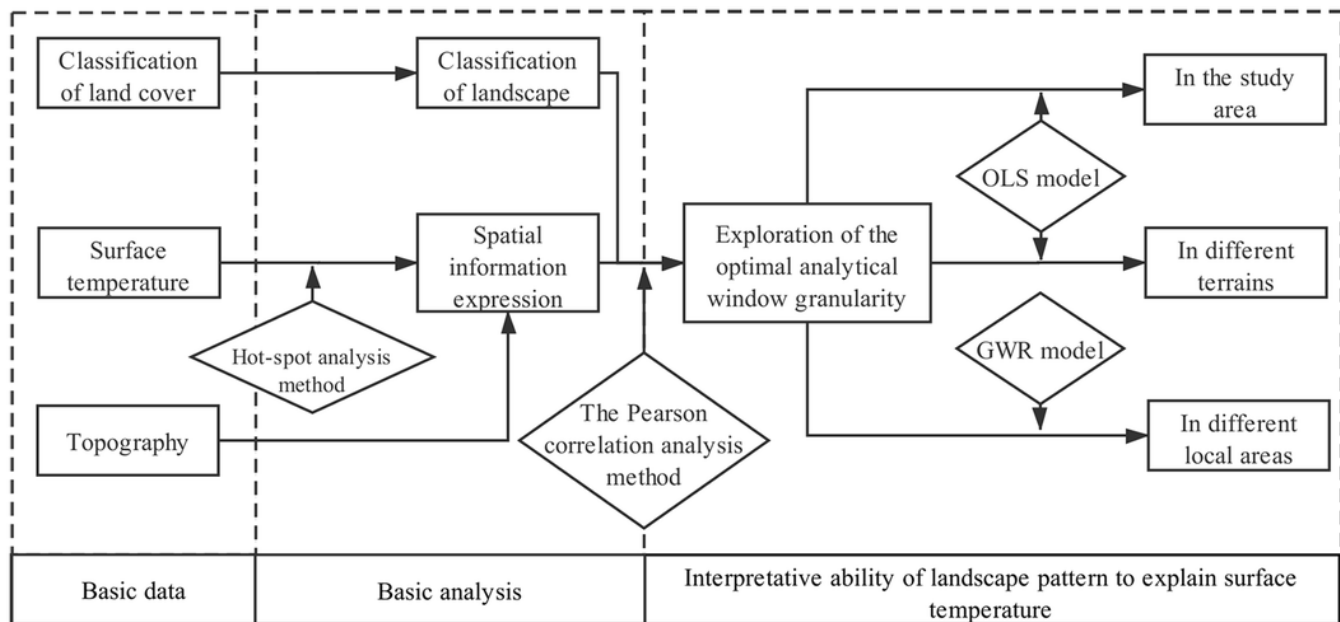
Figure 3

Figure 2 Terrains and elevation of the Beijing-Tianjin-Hebei urban agglomeration

In the figure, the purple line refers to the dividing line between different terrains, the different colors represent different elevation values. The gradient color legend and the classification of elevations distinguish the terrains including plains, hills, and plateau.
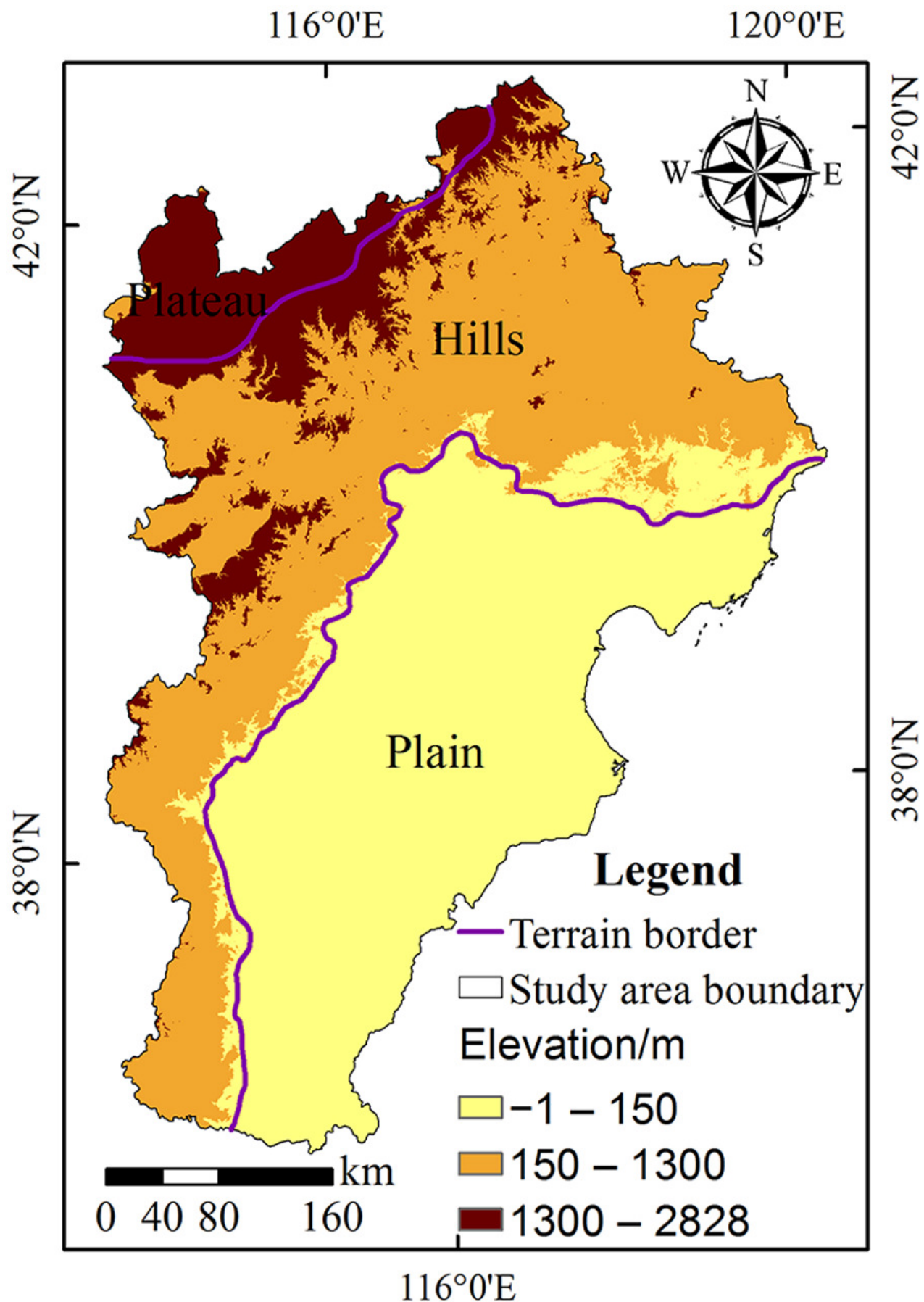
Figure 4

Figure.4 Spatial distribution of landscape

Dark green areas are ForLS, light green areas are GraLS, blue areas are WetlLS, yellow areas are FarmLS, red areas are ArtLS, and Brown areas are BareLS.
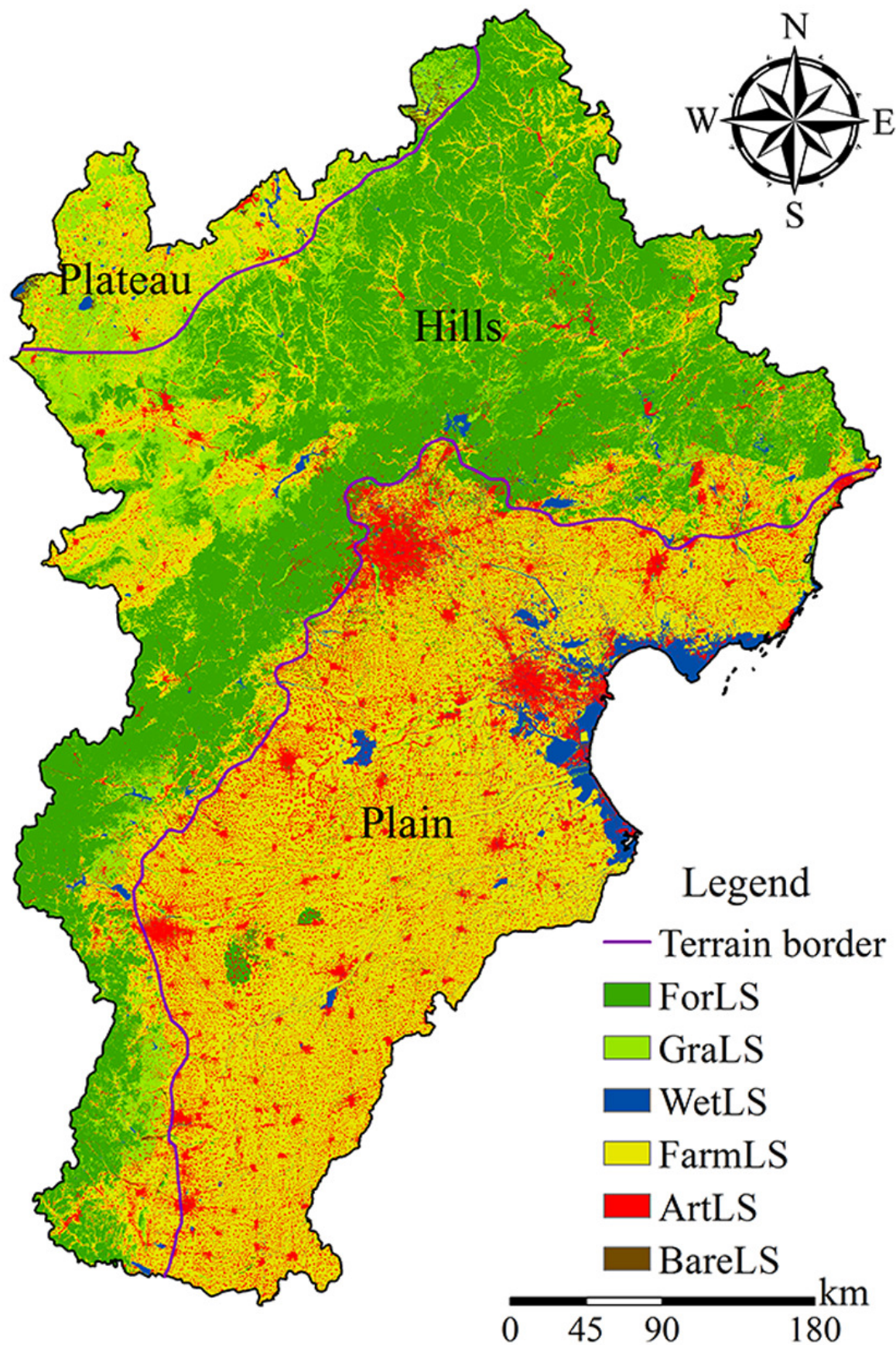
Figure 5

Figure.5 Hot-spot analysis of surface temperature

The blue area is the significant cold spot area of surface temperature, the red area is the significant hot spot area of surface temperature, and the blank area is the cold /hot spot area with no obvious concentration of surface temperature.
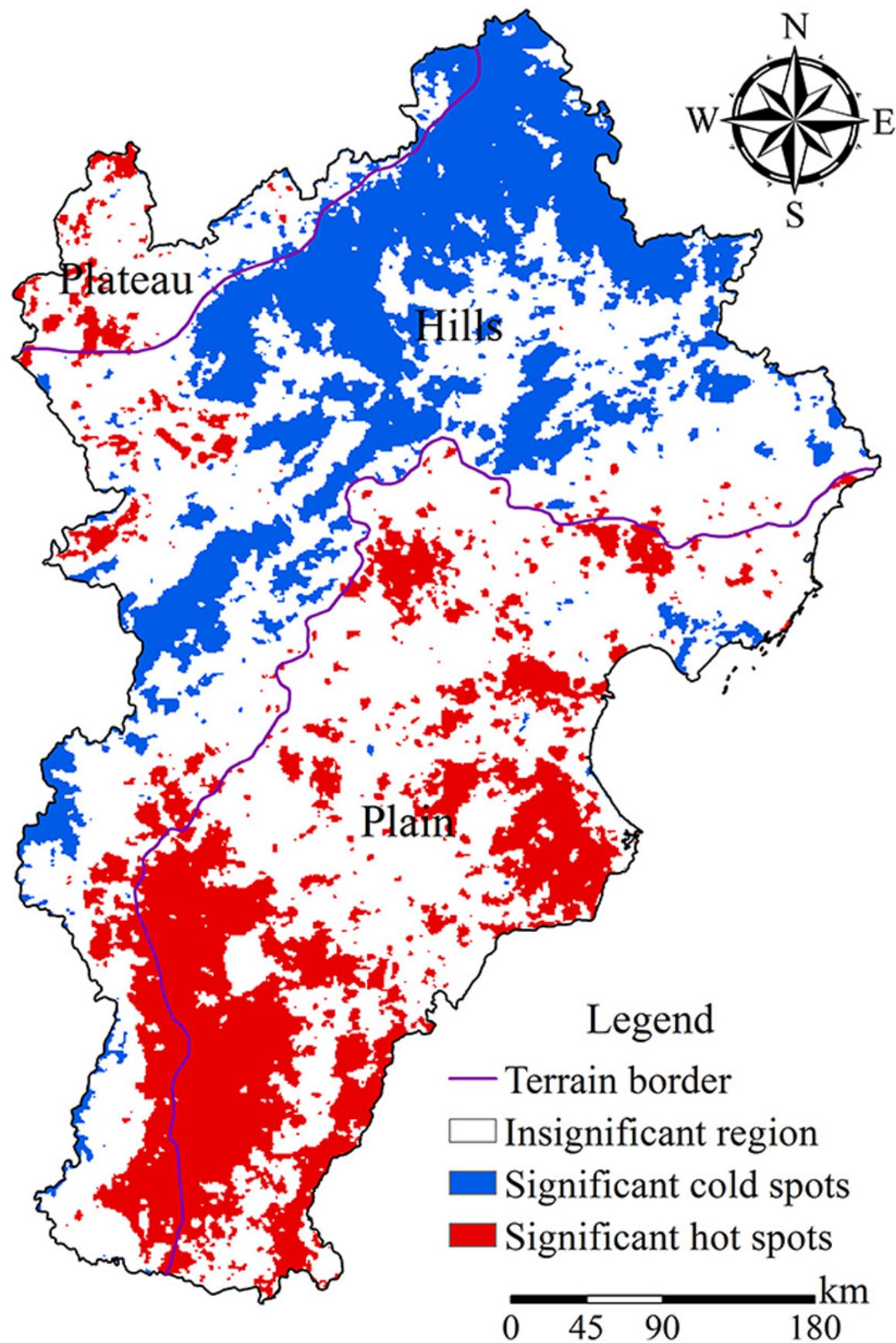
Figure 6

Figure.6 The square of Pearson correlation coefficient (r^2) based on different analytical window granularity

The black line represents ForLS, the red line represents GraLS, the blue line represents WetLS, the pink line represents FarmLS, the green line represents ArtLS, the dark blue line represents EcoLSP, and the purple line represents GreenLSP.
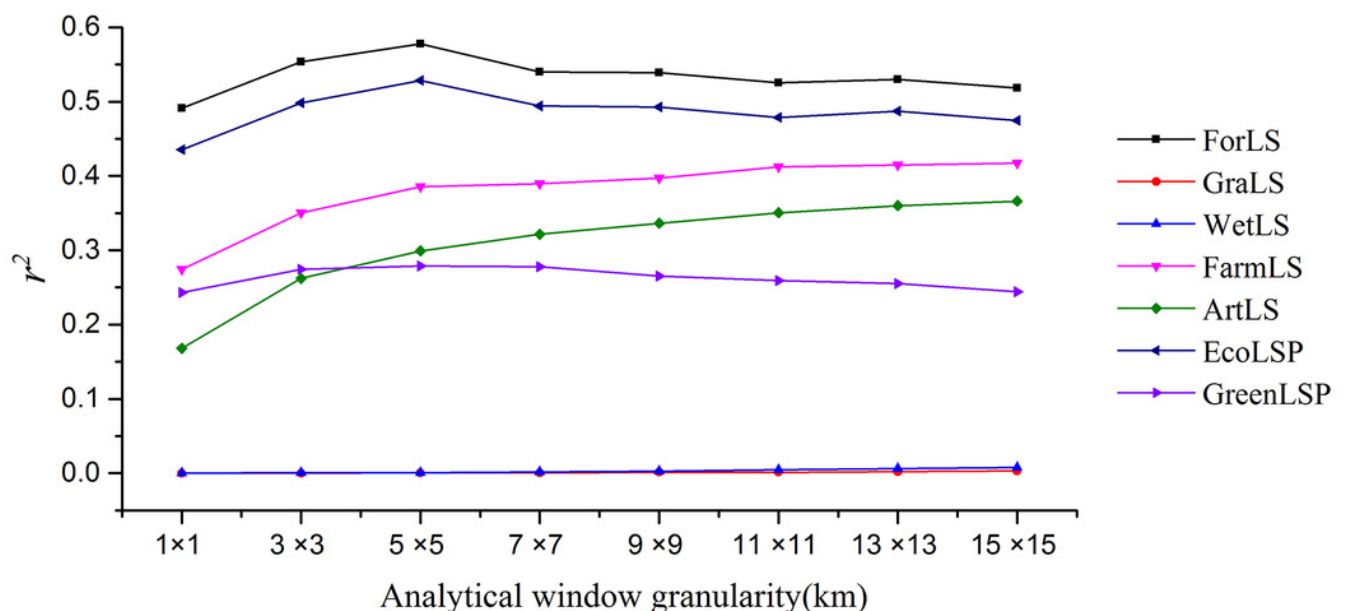
Figure 7

Figure.7 Results of the relationship between landscape pattern and surface temperature (R^2 and regression coefficient) using GWR: (A) EcoLSP and (B) GreenLSP and (C) FarmLS and (D) ArtLS.

(A) EcoLSP and (B) GreenLSP and (C) FarmLS and (D) ArtLS, and the darker the color, the greater the coefficient /R^2.